Realization of pressure sensor in ZnO semiconductor using the combination of photonic structure and FDTD method

C. S. MISHRA[1], M. R. NAYAK[2], S. K. TRIPATHY[3], R. N. SATPATHY[4], G. PALAI[4,*]
[1]*Department of ECE, Gandhi Institute for Technological Advancement (GITA), Bhubaneswar, India*
[2]*Department of Electrical Engineering, Centre for Advanced Post Graduate Studies, Biju Patnaik University and Technology, Odisha, Rourkela, India*
[3]*National Institute of Technology, Silchar, Assam, India*
[4]*Faculty of Science and Faculty of Emerging Technology, Sri Sri University, Cuttack, Odisha, India*

A two-dimensional square-shaped photonic crystal structure with a line defect is considered for pressure sensing application in the current research paper. The operational principle of the investigation of pressure explicitly relies on the field distribution in the defective region, which is made through the FDTD (finite difference time domain) method. Further, the intensities of the output signal are computed through an analytical treatment of the variation of the intrinsic parameter of the crystal. Ultimately, it is found that the amount of pressure exerted associated with the ZnO semiconductor is computed by knowing the intensity at the output end.

(Received April 29, 2022; accepted November 24, 2023)

Keywords: ZnO, Pressure, 2D photonic crystal, FDTD

1. Introduction

At present, nanophotonic devices play a key role in solving different problems in optical communication, nanoantenna, sensing etc [1]. Photonic crystal waveguide is used nowadays for the same. However, line defects in two-dimensional photonic waveguides may be utilised for pressure sensors by ZnO refractive index deviation [2]. Moreover, the output intensities of the PCs waveguide depend on parameters such as the dimension of the structure, the nature of the material and input wavelength for high bandwidth transmission [3]. The characteristics of ZnO substance have large bandgap spacing (3.37 eV) and a strong binding energy of 60 meV, for which ZnO is quite useful and finding an applications of skincare products. The applications of ZnO are also extended in the area like textile industry, photocatalyst, solar cells, pharmaceutical, cosmetics, rubber industries, biomedical sensors, and many others. ZnO exhibits more light absorption capability pertaining to Ultra Violet A (315–400 nm) and Ultra Violet B (280–315 nm) areas. When it comes to photonic crystal sensor applications, there are a few options such as sensing applications are identified as temperature sensors [4], optical fiber sensors [5], pressure sensors [6-7], planar waveguide sensors [8], strain sensors [9], laser-based sensor [10], sensor multiplexing and networking [11], and biophotonic sensors [12]. Again, the transmission and displacement field of two-dimensional photonic crystals have been discussed by employing the FEM method [13]. The transmitted signal arising from the photonic structure based on high pressure sensor is computed using several forms of losses [14, 16] and power amplification has been proposed by a 2D L-shaped photonic crystal [15]. However, different types of photonics-based pressure sensors have been discussed in different journals as well as articles, which are discussed in the literature reviews [4-16]. Further, a ring resonator based photonic pressure sensor has been discussed by employing both FDTD and FEM techniques [17]. Photonic based optical logic gate has been proposed[18] and quantum well-structure based 1D photonic crystal is discussed with a high pressure range[19] Temperature based optical switch has been proposed using a 2D photonic structure[20]. An optical encoder has been suggested by using a 2D photonic crystal ring resonator [21]. After analyzing recently published articles [17-21], we proposed a 2D photonic based L shaped structure for pressure sensing application. This paper presents a line defect waveguide of a square type 2D photonic pressure sensor, where the finite difference time domain is used to solve this problem.

2. Structure analysis

The proposed ZnO-based square type photonic crystal is arranged in the form of cylindrical rods, where Air is assumed to be the background material for pressure sensing an application. The periodic structure of ZnO-based photonic crystal is designed in 15×15 nanostructure cylindrical rods having lattice spacing (a) of 500 nm, which is constant during the computation of pressure. The defect in the waveguide is made by eliminating one line of rods (11th line of cylindrical rods) oriented in an L shape

direction, which is depicted in Fig. 1.

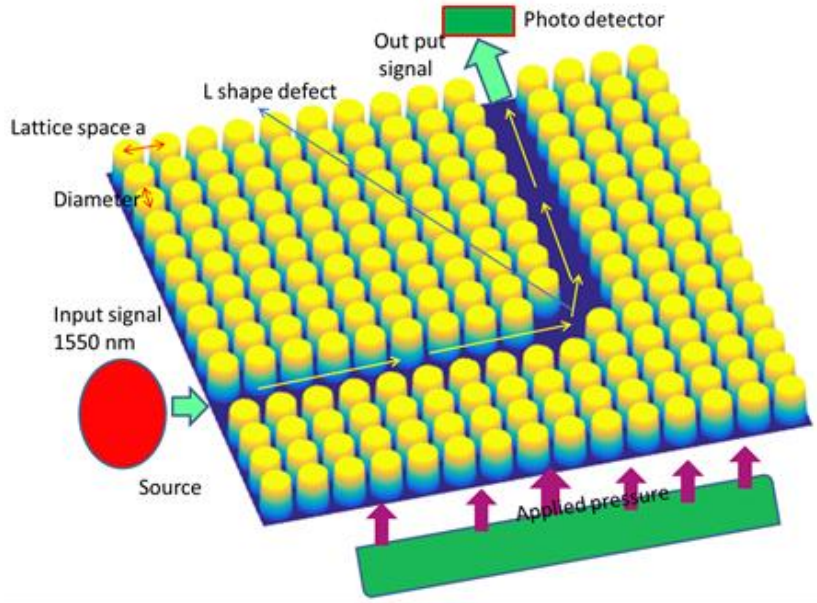

Fig. 1. Projected ZnO based 2D photonic structure for pressure sensor (color online)

The area of the configuration of the ZnO structure is 7.55 μm^2. Here the radius of ZnO crystal is taken as 200 nm, 210 nm, 220 nm, 230 nm, and 240 nm respectively, where lattice spacing is taken 500 nm for all types of computation. Similarly, dielectric constants of the ZnO photonic crystal are varied due to applied pressure, where applied pressures range from 0 GPa to 7 GPa. If the applied pressure varies, then the refractive index of the material structure changes accordingly.

3. Parameters of computational methods (FDTD)[26-27]

The Parameters of Computational Methods (FDTD) like Boundary Condition, Computational Domain, Space and Time Interval play a crucial role in simulating complex physical phenomena. A widely used technique in the realm of electromagnetics is the Finite-Difference Time-Domain (FDTD) method. FDTD is a numerical method that discretizes both time and space to simulate the behaviour of electromagnetic waves. To effectively employ FDTD, it is essential to carefully define and set several key parameters, including boundary conditions, computational domain, space and time intervals. These parameters significantly influence the accuracy, efficiency, and applicability of FDTD simulations.

a) Boundary Conditions: Boundary conditions are essential to define how electromagnetic fields behave at the edges of the computational domain. There are different types of boundary conditions in FDTD, it includes

Perfectly Matched Layer (PML): PML is a widely used absorbing boundary condition that minimizes reflections from the edges of the simulation domain.

Periodic Boundary Conditions: These conditions are used to simulate an infinite space by wrapping the field values around the edges of the computational domain.

Electric or Magnetic Boundary Conditions: These are used when dealing with specific problems like waveguide simulations, and they prescribe the behaviour of electric or magnetic fields at the boundary. The choice of boundary conditions depends on the specific problem being simulated and the desired accuracy of the results.

b) Computational Domain: The computational domain is the region in which the electromagnetic fields are simulated. It should encompass the entire region of interest where electromagnetic phenomena are being studied. The size and shape of the computational domain must be chosen carefully to ensure that the results are accurate and that there are no unwanted reflections from the boundaries. It is also essential to strike a balance between the size of the domain and the computational resources required

c) Space and Time Interval: FDTD discretizes both space and time. These discretization intervals, often denoted as Δx (spatial) and Δt (temporal), determine the resolution of the simulation and directly affect its accuracy and efficiency. Smaller intervals result in higher accuracy but require more computational resources and longer simulation times. The choice of these intervals must consider the Courant-Friedrichs Lewy (CFL) stability condition, which sets a limit on the ratio of Δx to Δt to ensure numerical stability.

Spatial Interval (Δx): Smaller values of Δx lead to a finer grid, allowing for better representation of small-scale features and high-frequency phenomena.

Temporal Interval (Δt): Smaller values of Δt enable the accurate tracking of rapid changes in the electromagnetic fields. The choice of Δx and Δt should strike a balance between accuracy and computational cost.

The parameters of computational methods like FDTD, including boundary conditions, computational domain, and space and time intervals, are critical aspects of electromagnetic simulations. These parameters must be carefully selected to achieve accurate and efficient results for specific problems. Additionally, adapting these parameters to the problem at hand and the available computational resources is essential for the successful application of the FDTD method in various fields such as antenna design, sensing application of photonic crystals, networking, optical communication systems, wave propagation studies, and electromagnetic compatibility analysis.

4. Relation of refractive index to pressure for ZnO[28-29]

The refractive index of a material like zinc oxide (ZnO) can be influenced by various factors, including pressure. In general, the refractive index of a material can be expressed as a function of its intrinsic properties and external conditions. The refractive index, often denoted as "n" of a material like ZnO can be represented as:

$$n(P, T) = n_0 + \partial n/\partial P * \Delta P + \partial n/\partial T * \Delta T \quad (1)$$

where n(P, T) is the refractive index at a given pressure (P) and temperature (T). n_0 is the refractive index at standard conditions (typically at atmospheric pressure and room temperature).$\partial n/\partial P$ is the change in refractive index with respect to pressure. $\partial n/\partial T$ is the change in refractive index with respect to temperature.ΔP is the change in pressure from standard conditions. ΔT is the change in temperature from standard conditions. The refractive index of ZnO can change with pressure, particularly at high pressures. This effect is a result of changes in the material's electronic structure and its response to compression. To precisely determine the relationship between refractive index and pressure for ZnO, experimental data and equations of state for the material under different pressure conditions would be required.

5. Effect on the refractive index of air with pressure[30-31]

In the case of air, the refractive index is influenced by changes in pressure and temperature, primarily due to the ideal gas law and its impact on the density of air. The refractive index of air, often denoted as "n_air," can be described using the Gladstone-Dale relation:

$$n\_air = 1 + (N * \Delta P) / (\lambda * P1) \quad (2)$$

where n_air is the refractive index of air. N is the number of molecules per unit volume (number density) of air. ΔP is the change in pressure. λ is the wavelength of light. P1 is the pressure at standard conditions.

Changes in pressure (ΔP) can indeed affect the refractive index of air. However, the effect is relatively small for typical atmospheric pressure variations. In precision optics and metrology, corrections are often made for variations in air refractive index caused by changes in pressure and temperature to ensure accurate measurements. The refractive index of materials like zinc oxide (ZnO) can be influenced by pressure, but the precise relationship would require experimental data. In the case of air, there is an effect on the refractive index with changes in pressure, although it is generally small and corrected for in precise measurements.

6. Result analysis

Fig. 1 illustrates the pictorial representation of the 2D photonic waveguide realized as a sensor of pressure. The input wavelength of 1550 nm from a laser source is incident to the waveguide to fetch the amount of pressure. Here the radius of the ZnO rod and the applied pressure of structural changes constantly. The range of pressure and the radius of the cylindrical rods are taken from 0 GPa to 7 GPa and 200 nm to 240 nm respectively. Here the signal propagates along the 90-degree bend path (11th line defect) of the waveguide. The physics of the work depends on the refractive index of the background material related to the pressure. For example, different pressure acting on the ZnO material leads to the different values of refractive indices. The refractive index of ZnO of pressure 1 GPa is not the same as the pressure of 7 GPa. The peak of the electric field distribution has been evaluated at the output end of the photonic waveguide, which is computed through the FDTD method. The simulation has been conducted for all cylindrical radii ranging from 200 nm to 240 nm and amount of pressure variation of 0 GPa to 7 GPa respectively. Though it has performed many simulations by changing the said parameters, only one sample (radius 240 nm and pressure 7 GPa) is provided and made available in Fig. 2. In this graph, the peak of the electric field distribution for the same is found to be 0.4548 V/μm.

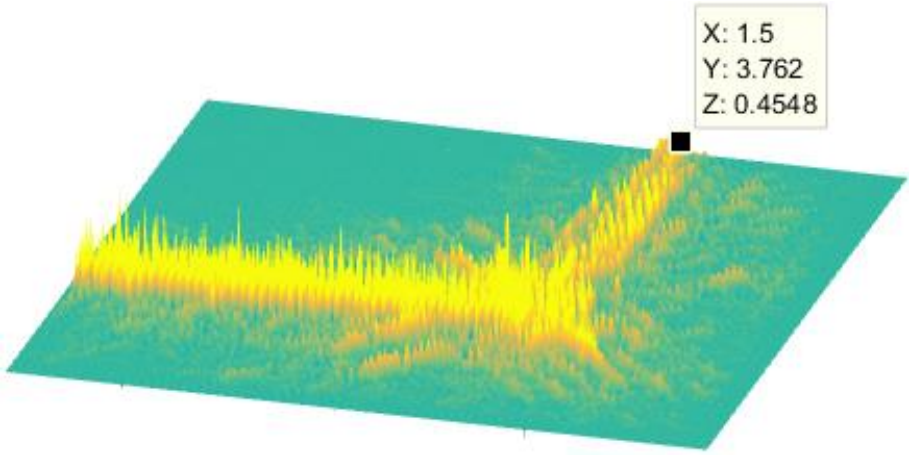

Fig. 2. Electric distribution of radius 240 nm at applied pressure 7 GPa (color online)

Considering similar techniques, the peak electric field at the output end is found and the output result is indicated for all pressures in Table 1. The detailed information of radius, pressure, and peak electric field is shown in the below table.

Table 1. Electric field distribution with regard to the pressure and radius (lattice spacing 500 nm)

Pressure (GPa)	0	1	2	3	4	5	6	7
Radius (nm)	Electric field(Peak) in V/μm	Electric field(Peak) V/μm	Electric field(Peak) V/μm	Electric field(Peak) V/μm	Electric field(Peak) V/μm	Electric field(Peak) V/μm	Electric field(Peak) V/μm	Electric field(Peak) V/μm
200	0.1764	0.1666	0.2674	0.2619	0.4262	0.4281	0.242	0.1985
210	0.1704	0.1562	0.1596	0.138	0.2281	0.1773	0.1416	0.2188
220	0.1156	0.1372	0.6469	0.6138	0.2872	0.3169	0.6191	0.5475
230	0.3701	0.3569	0.3152	0.4099	0.3735	0.2741	0.3586	0.2413
240	0.9831	0.5126	0.5963	0.8551	0.3632	0.492	0.3746	0.4548

Since the principle of investigation depends on the variation of electric field distribution, fetched from Table 1, it has been observed that the deviation of the peak electric field with respect to the pressure follows a non-linear trend. It is confirmed that the proposed structure exhibits non-linearity due to the Kerr effect. So the output intensity pertaining to each electric field could be realised through non-linear phenomena. Let us discuss it. Further, with the help of equations number (4) and (5) where the intensities corresponding to each pressure are obtained pertaining to the different dimensions of the cylindrical rod. The resultant intensity of the proposed ZnO-based photonic structure is shown in Fig. 3.

In Fig. 3, the pressure in GPa has been chosen along the x-axis, and intensity of light in microW/m^2 is placed along the y-axis, which is shown in Fig. 3. The characteristics of the graph clearly suggested that intensity varies non-linearly with an incremented value of applied pressure. For example, the output intensities of constructed photonic device fluctuate from 8.67 mW/m^2 to 10.71 mW/m^2, 8.09 mW/m^2 to 13.02 mW/m^2, 3.72 mW/m^2 to 81.53 mW/m^2, and 269.55 mW/m^2 to 56.26 mW/m^2 for the radius of 200 nanometre, 210 nanometre, 220 nanometre, and 230 nanometre, 240 nanometre respectively. Following a thorough investigation of the above work, it has been realised that 5 kinds of the value of output intensity, one can measure the amount of pressure associated with it.

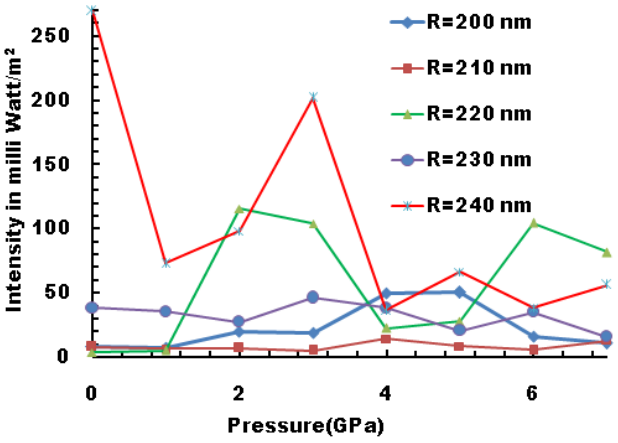

Fig. 3. Pressure and output intensity of PCW (15x15) with line defect waveguide with the variation of radius (color online)

The transportation of signal through the photonic waveguide is generated where Maxwell equations inevitably are the source. The field distribution referred to as photonic crystal waveguide is originated from the curl and the dot product of Maxwell's electromagnetic equations. The relationship among the electric flux density, the electric field, and polarization field is written as

$$D_1 = \varepsilon_0 E_1 + P_1 \tag{3}$$

where D_1, ε_0, E_1, P_1 are displacement, permittivity, electric field and polarization respectively. The generated polarization P_1 of nonlinear photonic crystal medium is obtained as a function of the susceptibility coefficients [22-25]

$$P_1 = \varepsilon_0 E_1 S^{(1)} + \varepsilon_0 {E_1}^2 S^{(2)} + \varepsilon_0 {E_1}^3 S^{(3)} \tag{4}$$

where $S^{(1)}$, $S^{(2)}$, and $S^{(3)}$ are the susceptibility coefficients of 1st, 2nd, and 3rd order. Now the device configurations do not possess second order susceptibility ($S^{(2)}$), which is observed in non-centrosymmetric photonic crystals. The 3rd order susceptibility coefficients ($S^{(3)}$) perform for both non-centrosymmetric and centrosymmetric medium and the projected photonic crystal structures explain this susceptibility due to Kerr nonlinearity.

For the monochromatic electric field, the produced polarisation (P1) of the medium might be stated, $E_1=E_1(t)\cos\omega t$ is

$$P_1 \approx \epsilon_0 (S^{(1)} + \frac{3}{4} S^{(3)} |E_1|^2 E_t \cos\ \omega t \tag{5}$$

Also, with consideration of the subsequent susceptibility as a sum of nonlinear and linear terms, the energy of light can be expressed as

$$\text{Energy}_O = n_0 + \frac{3S^{(3)}}{8n_0} \times |E_1|^2 \tag{6}$$

Further intensity can be determined by

$$\text{Intensity=Energy/Area} \tag{7}$$

In Fig. 4, the output intensity in milliwatt/meter square has been chosen along the x-axis and the input intensity of light in kW/m^2 is placed along the y-axis, which is shown in Fig. 4. The characteristics of the graph clearly suggested that intensity varies non-linearly with an incremented value of input intensity. For example, the input intensities of constructed photonic device fluctuate from 234.22 kW/m^2 to 337.28 kW/m^2 for the radius of 200 nanometre, 210 nanometre, 220 nanometre, and 230 nanometre and 240 nanometre respectively.

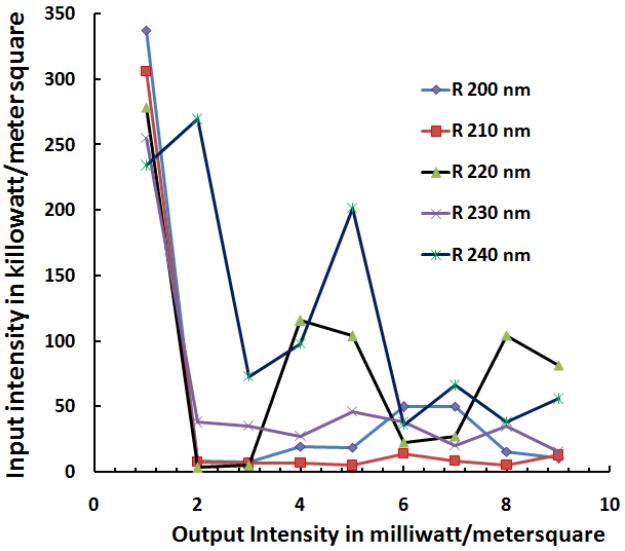

Fig. 4. Input intensity and output intensity of PCW (15x15) with line defect waveguide with the variation of radius (color online)

In nonlinear optical studies, the input intensity of light and the nonlinearity introduced play crucial roles in understanding the behavior of a material or system. The input intensity of light refers to the power or energy per unit area of a light beam that is incident upon a material or device. It is typically measured in units like watts per square meter (W/m^2). We vary the input intensity of the incident light to investigate how a material or system responds differently as the intensity increases, which depends on the defective area of the structure. Nonlinearity in optics occurs when the response of a material to light is not directly proportional to the intensity of the incident light. This nonlinearity can manifest in various ways, such as the optical Kerr effect, two-photon absorption, or other nonlinear processes. The nonlinearity is typically characterized by a parameter called the nonlinear coefficient, which quantifies how the material's optical properties change as a function of input intensity. We plot the input intensity of light against the output intensity. This graph helps visualize how the material's response deviates from a linear relationship as the input intensity increases.

7. Conclusion

The pressure sensor is realized in this article through the analysis of the non-linear effect of the photonic crystal waveguide. The principle of investigation relies on the non-linear variation of electric field distribution pertaining to both structure configuration and external pressure. The electric field distribution is estimated through the analysis of the finite difference time domain approach. The output results relating to intensity and pressure variation indicate that intensity varies non-linearly with pressure at different structural configurations. Finally, one can know the amount of pressure exerted on the waveguide by knowing the value of intensity.

References

[1] J. D. Joannopoulos, R. D. Meade, J. N. Winn, Photonic Crystals: Molding the Flow of Lights Princeton University Press, Princeton, 1995.

[2] A. R. Goni, F. Kaess, J. S. Reparaz, M. I. Alonso, M. Garriga, G. Callsen, M. R. Wagner, A. Hoffmann, Z. Sitar, Physical Review B **90**, 045208 (2014).

[3] I. A. Sukhoivanov, I. V. Guryev, Physics and Practical Modeling: Photonic Crystals, Springer, Heidelberg, 2009.

[4] C. S. Mishra, G. Palai, Optik **137**, 37 (2017).

[5] A. David Krohn, Trevor W. MacDougall, Alexis Mendez, Fiber Optic Sensors: Fundamentals and Application, fourth edition, WA: SPIE Press, Bellingham, 2015.

[6] S. Olyee, A. A. Dehghani, Photon Sensors **2**, 92 (2012).

[7] C. S. Mishra, A. Nayyar, S. Kumar, B. Mahapatra, G. Palai, Optik **176**, 56 (2019).

[8] M. A. Butt, S.N. Khonina, N. L. Kazanskiy, CEUR Workshop Proc. **1638**, 16 (2016).

[9] Tsan-Wen Lu, Chia-Cheng Wu, Po-Tsung Lee, ACS Photonics **5**, 2767 (2018).

[10] https://www.photonics.com/Articles/LaserBased_Sensor_Simplifies_Improves_Benzene/a66486.

[11] E. Achaerandio, S. Jarabo, S. Abad, M. Lopez-Amo, IEEE Photonics Technology Letters **11**, 1644 (1999).

[12] Z. Gharsallah, M. Najjar, B. Suthar, V. Janyani, Optical and Quantum Electronics **50**, 249 (2018).

[13] Guilin Wen, Haifeng Ou, Jie Liu, Materials Today Communications **24**, 100977 (2020).

[14] C. S. Mishra, M. R. Nayak, S. K. Sahu, G Palai, Optoelectron. Adv. Mat. **15**(9-10), 420 (2021).

[15] Chandra Sekhar Mishra, Optical Materials **127**, 112298 (2022).

[16] C. S. Mishra, S. R. Mondal, R. Arunachalam, M. R. Nayak, S. K. Tripathy, G. Palai, Optical and Quantum Electronics **55**(1), 33 (2023).

[17] Uttara Biswas, J. K. Rakshit, B. Suthar, D. Kumar, C. Nayak, International Journal of Numerical Modelling: Electronic Networks, Devices and Fields **35**(2), e2962 (2022).

[18] Mayur K. Chhipa, B. T. P. Madhav, S. Robinson, V. Janyani, B. Suthar, Optical Engineering **60**(7), 075104 (2021).

[19] Suthar Bhuvneshwer, Anami Bhargava, Silicon **13**(6), 1765 (2021).

[20] Mayur K. Chhipa, B. T. P. Madhav, B. Suthar, Journal of Computational Electronics **20**, 419 (2021).

[21] Mayur Kumar Chhipa, B.T.P. Madhav, B. Suthar, V. Janyani, Photonic Network Communications **44**(1), 30 (2022).

[22] Richart E. Slusher, Nonlinear photonic crystals, Springer, New York, 2003.

[23] I. A. Sukhoivanov, I. V. Guryev, Photonic Crystals: Physics and Practical Modeling **152**, Springer, Heidelberg, 2009.

[24] C. S. Mishra, A. Nayyar, G. Suseendran, G. Palai, Optik **178**, 509 (2019).

[25] C. S. Mishra, G. Palai, D. Prakash, S. K. Tripathy, K. D. Verma, Optik **144**, 522 (2017).

[26] Natalia K. Nikolova, W. Tam Helen, H. Bakr Mohamed, IEEE Transactions on Microwave Theory and Techniques **52**(4), 1207 (2004).

[27] Timothy Van Renterghem, Erik Salomons, Dick Botteldooren, Applied Acoustics **67**(6), 487 (2006).

[28] E. Şenadim Tüzemen, H. Kavak, R. Esen, Physica B: Condensed Matter **390**(1-2), 366 (2007).

[29] M. Mekhnache, A. Drici, L. Saad Hamideche, H. Benzarouk, A. Amara, L. Cattin, J. C. Bernède, M. Guerioune, Superlattices and Microstructures **49**(5) 510 (2011).

[30] Bengt Edlén, Metrologia **2**(2), 71 (1966).

[31] James C. Owens, Applied Optics **6**(1) 51 (1967).

*Corresponding author: gpalai28@gmail.com